Charles C Watson, Vladimir Y Panin, Sune H Keller, Søren Holm, Johan Nuyts. "A sparse transmission method for PET attenuation correction in the head", *IEEE NSS MIC*, Seattle, WA, USA, 2014. M14-4.

A Sparse Transmission Method for PET Attenuation Correction in the Head

Charles C Watson *Senior Member, IEEE,* Vladimir Y Panin *Member, IEEE,*
Sune H Keller *Member, IEEE,* Søren Holm, and Johan Nuyts

***Abstract*—We describe a novel solution for PET attenuation correction in the head based on the joint reconstruction of simultaneously acquired emission and sparse transmission (sTX) data. We demonstrate that an sTX array can provide better cross-talk reduction than a conventional full-ring transmission source. This initial evaluation is based on synthetic 2D non-time-of-flight data corresponding to 20 fixed line sources placed in a 30 cm diameter ring around the head. A 57.2 cm ring diameter is also considered. The total source activity equals half the total emission activity in the brain. Simultaneous emission/transmission and blank scans are simulated. These data are iteratively reconstructed to estimate both the emission and linear attenuation coefficient (LAC) images of the head. We find that the sTX data effectively constrain cross-talk. Bone, soft tissue and voids are approximately represented in the estimated attenuation image. The results are compared to a continuous ring-source-based joint reconstruction, as well as to a standard MLEM reconstruction of emission-only data assuming a uniform linear attenuation coefficient (LAC) distribution within the head. 10–20% underestimation of activity in the peripheral regions of the brain in the latter two images is reduced to $< 5\%$ on average in the sTX case. Initial tests indicate the algorithm is robust to a realistic level of noise. We estimate that such an sTX technique would result in a negligible increase in patient absorbed radiation dose in a typical ^{18}FDG clinical study of the head.**

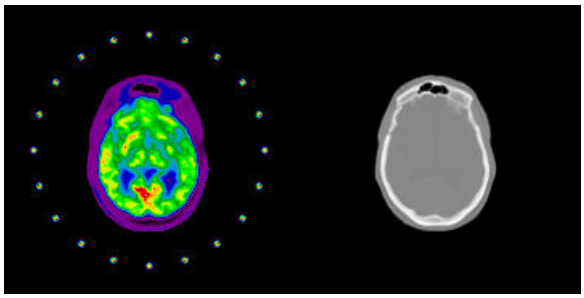

Fig. 1. Left: EM+sTX image. Right: CT-derived LAC image.

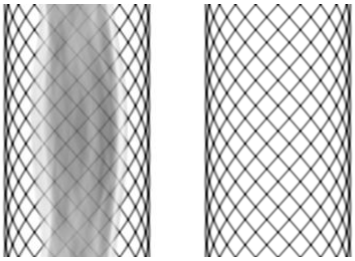

Fig. 2. Left: EM+sTX sinogram. Right: Blank sinogram.

I. Introduction

Quantitative PET neurological imaging requires accurate attenuation correction (AC). For applications where patient-specific CT-based AC is not available or desirable, several alternative solutions have been employed [1]. These include the joint estimation of activity and attenuation from emission-only data (MLAA) [2], MR image segmentation [3], [4], and CT/MR atlas-based approaches [5], [6]. In [7] we demonstrated that in some cases the use of a few fixed transmission sources in a simultaneous emission-transmission acquisition and joint reconstruction could significantly improve the accuracy of attenuation correction compared to using emission data only. In related work, Erdoğan and Fessler [8] proposed an algorithm for the joint estimation of activity and attenuation from separate post-injection transmission and emission-only scans. Panin *et al.* [9] evaluated an algorithm for the joint reconstruction of simultaneously acquired emission and transmission data in torso-like phantoms using a rotating rod source and time-of-flight (TOF) data. In this paper we explore the potential of a sparse transmission system for PET imaging of the head. We jointly reconstruct emission (EM) and linear attenuation coefficient (LAC) images from simultaneously acquired emission-transmission data using an alternating iterative algorithm [7] similar to those discussed in [2] and [9]. The initial evaluation presented in this paper is based on 2D reconstruction of non-TOF synthetic data derived from actual CT and PET clinical images. Potential applications of the technique include integrated PET/MR systems and low-dose stand-alone PET scanners for diagnosis of Alzheimer's dementia.

Manuscript received November 30, 2014.

C Watson and V Panin are with Siemens Healthcare, Knoxville, TN 37932 USA (telephone: +1.865.218.2000, e-mails: charles.c.watson@siemens.com, vladimir.panin@siemens.com).

S H Keller and S Holm are with the Department of Clinical Physiology, Nuclear Medicine and PET, Rigshospitalet, Copenhagen University Hospital, Copenhagen, Denmark (emails: Sune.Hoegild.Keller@regionh.dk, Soeren.Holm@regionh.dk).

J Nuyts is with the Department of Nuclear Medicine, K.U. Leuven, B-3000 Leuven, Belgium (e-mail: johan.nuyts@uzleuven.be).

II. Methods

Fig 1 shows axial slices through ^{18}FDG emission and CT-derived LAC brain images that are the ground truth for our simulation. Also shown in the emission image is a circular array of 20 discrete line sources at a radius of 15 cm from the center of the field-of-view (FOV). These images were forward projected and attenuation was applied to generate a simultaneous emission plus sparse transmission (EM+sTX) sinogram.

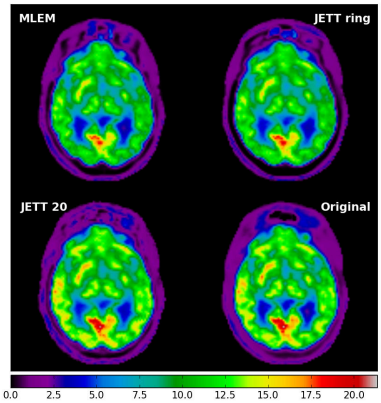

Fig. 3. EM reconstructions versus original. Units are kBq/ml.

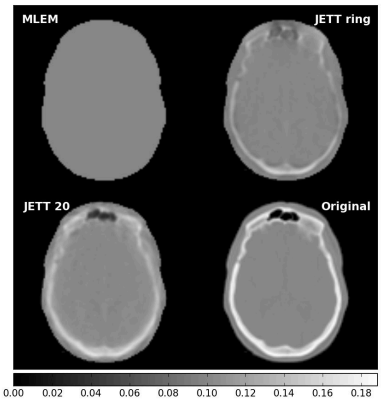

Fig. 4. LAC images versus original. Units are cm^{-1}.

An emission-only (EM) sinogram was also projected. Scatter and randoms were not modeled, and the attenuation of a head holder or other fixtures was not considered. A blank sinogram (no object in the FOV) was formed by projecting the sTX array only. The EM+sTX and blank sinograms, shown in Fig 2, are the synthetic data from which we wish to estimate the images in Fig 1. We have investigated arrays of 3–32 sources, with each source having emission activity between 1 and 5% of the total brain activity. Here we present results for 20 sources with 2.5% activity, although the true optimal configuration has not yet been determined. We compare these results to a conventional full ring source having the same diameter and total activity. To assess the effect of source position, we repeated the simulation using a larger source ring radius of 28.6 cm.

An alternating iterative reconstruction algorithm similar to MLAA was used [2], [7], [9]. The emission update step is:

$$\lambda^{n+1} = \frac{\lambda^n}{P_-[\alpha^n]} P_- \left(\frac{y}{P_+[\lambda^n] + b} \right) \tag{1}$$

and the attenuation update is:

$$\mu^{n+1} = \mu^n + \frac{\beta}{N} \left(1 - \frac{P_-[y]}{P_-[\alpha^n (P_+[\lambda^{n+1}] + b)]} \right) \tag{2}$$

where n is the iteration number, $\alpha^n = \exp(-P_+[\mu^n])$ is the sinogram of attenuation factors, μ is the LAC image, y is the EM+sTX sinogram, b is the blank sinogram, λ is

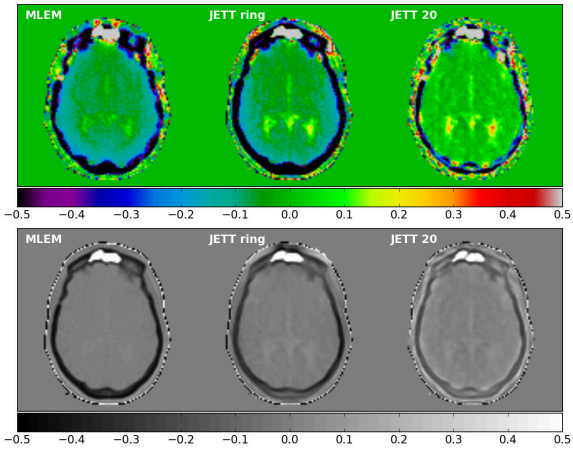

Fig. 5. EM (top) and LAC relative differences versus original, for the first axial slice. Clipped at ± 0.5.

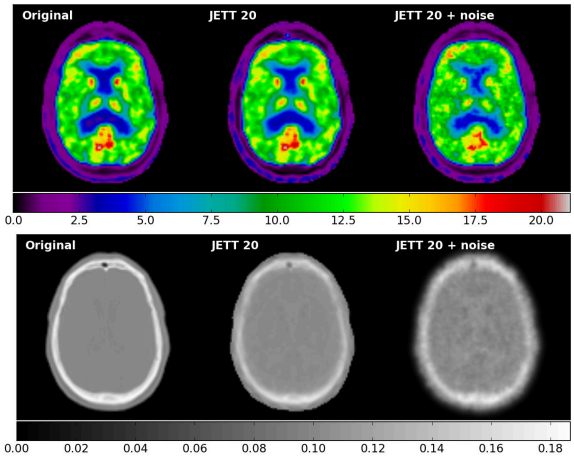

Fig. 6. EM (top) and LAC images reconstructed with and without noise, for the second axial slice. Units are kBq/ml and cm^{-1} respectively.

the emission image, β is a relaxation factor (2.0), N is the linear dimension of the image in pixels (281), and P_+ and P_- are forward and back-projectors respectively. We refer to this algorithm as Joint Emission and Transmission Tomography (JETT). The essential difference between JETT and standard MLAA is the introduction of the blank scan as if it were part of the forward model of the data. Correspondingly, the sTX sources themselves are not forward or back projected during the iteration.

The images are reconstructed within a mask region defined by the boundary of the CT-LAC image at a threshold of 0.015 cm^{-1}. The initial LAC image has a uniform value of 0.1 cm^{-1} within a slightly smaller region defined by thresholding at 0.05 cm^{-1}. In practice, a suitable convex envelope of the head could be pre-determined from the EM+sTX data. 200 iterations are performed. No prior probability constraints are used. Cross-talk is particularly problematic in low activity regions, but is significantly reduced by performing several MLEM iterations of the EM image before beginning the updates of the LAC image [2]. Here we have used 50 such pre-iterations. The sTX JETT results are compared to the

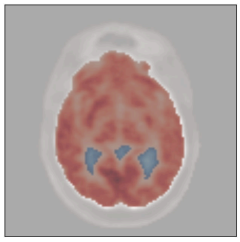

Fig. 7. The hot ROI is shown in red, and the disjoint cold one in blue.

TABLE I
RELATIVE ERRORS (%)

	MLEM	sTX		Ring TX	
		15 cm	28.6 cm	15 cm	28.6 cm
Hot Bias	-9.6	0.7	-0.8	-8.5	-8.7
Cold Bias	1.7	12.8	11.5	4.7	3.6
EM RMS	11.5	4.0	4.0	10.4	10.8
LAC RMS	23.9	14.3	16.2	19.8	21.5

ring-source based JETT reconstruction at the same number of iterations, as well as to a standard MLEM reconstruction of the EM-only sinogram, using the uniform LAC image for attenuation correction.

An initial test of robustness to noise was performed by adding Poisson deviations to the synthetic data for a second axial slice. The noise level was based on the (3D) clinical acquisition, from which we estimated 1.6e6 noise equivalent counts per image plane. The reconstruction was regularized by applying a 1.7 mm FWHM Gaussian smoothing filter to both the EM and LAC image estimates between iterations [10].

In order to assess performance more quantitatively, we have computed the relative root mean square (RMS) error in the EM and LAC images, as well as the mean relative bias in hot and cold regions of the emission images, determined by thresholding the image at 5 kBq/ml. The resulting regions of interest (ROIs) will be shown later in Fig 7. The mean activity values in the two regions were 11.0 and 4.1 kBq/ml. The mask used for computing the RMS emission error was the sum of these two ROIs, with a mean value of 10.7 kBq/ml. The mask used for the LAC RMS error calculation included the entire initial LAC image estimate as will be shown in Fig 4.

III. RESULTS

Fig 3 compares the three reconstructed EM images for the first axial slice to the original one on a global color scale. JETT 20 refers to the discrete source configuration. Fig 4 compares the corresponding LAC images. Fig 5 shows the EM and LAC image errors relative to the original images (e.g., MLEM/Original – 1). Note that in the frontal sinus, where the original EM and LAC image values are zero in most pixels, but the estimated image values are finite, the relative error is not defined. For these pixels we have set the relative error value to > 0.5 so that they appear at the highest value in the color scale. Fig 6 compares the noisy and noise-free JETT reconstructions to the original image for the second axial slice. The ROIs used for the emission image bias calculations are shown in Fig 7.

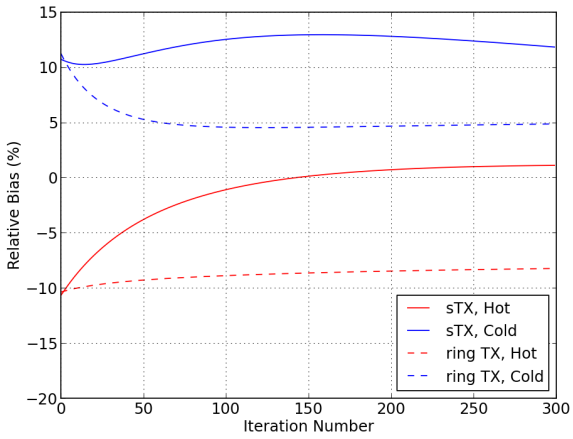

Fig. 8. Relative biases in the hot and cold ROIs as a function of iteration number, for the 15 cm ring and sTX cases.

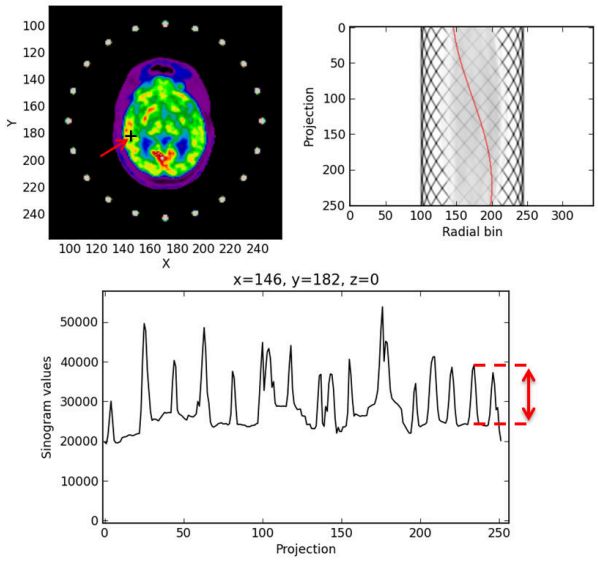

Fig. 9. A point in the brain, indicated by the cross in the upper left panel, corresponds to the red sinusoid through the EM+sTX sinogram as shown in the upper right panel. The profile through the sinogram along this sinusoid is plotted in the lower panel, where the red interval indicates the contribution of attenuated TX data.

Table I gives the relative error values corresponding to the four metrics evaluated. In Fig 8 we show the relative biases in the hot and cold ROIs versus iteration number for the 15 cm ring TX and sTX cases to indicate the degree of convergence achieved. The results reported in Table I are for 200 iterations.

IV. DISCUSSION

MLEM with a uniform LAC image produces a radial gradient in the EM image with 10–20% underestimation of activity in the peripheral regions of the brain due to the lack of attenuation correction for bone, as is known from clinical studies [11]. Although not shown here, we have found that unconstrained non-TOF MLAA (no TX) does not significantly reduce these errors. On the other hand, we find that simultaneous emission plus sparse transmission data with joint reconstruction reduces the peripheral brain activity errors

to 5% or less on average, although bias increases somewhat in the low-activity central regions. JETT approximately resolves bone and void regions in the LAC image. While it can be seen in Figs 4 and 5 that JETT 20 does not estimate the full amplitude of bone attenuation, it compensates for this to some extent by increasing the LAC values in the interior of the head slightly, particularly in the vicinity of the skull. The sinogram data consistency with JETT 20 (not shown) is consequently very good despite the residual errors in the LAC image.

The cold emission ROI results in Table I are surprising at first glance because they show that MLEM has the smallest residual bias. This is reminiscent of the clinical result that the colder regions near the center of the brain tend to have better SUV accuracy than the hot regions toward the periphery [11]. We believe this is coincidental, and occurs because the under-correction for attenuation in the head just happens to balance the under-convergence of the reconstruction in this region. In the reconstructions with more accurate attenuation correction, the under-convergence has a bigger effect.

Somewhat surprisingly, we find that the sparse TX array significantly outperforms the full-ring TX source (Fig 5). We believe this happens because having both EM-only and EM+TX data among the lines of response along the sinusoid corresponding to each image pixel helps resolve the emission versus attenuation ambiguity that leads to cross talk. This mechanism is illustrated in Fig 9: along the sinusoid profile the 'valleys' correspond to emission-only data, while the 'peaks' correspond to emission plus transmission data. The difference, shown by the red interval, is sensitive only to the attenuation of the head. Since the activity and LAC values in the pixel must be chosen to match both types of data, their effects are approximately decoupled. The decoupling is not exact since these two types of data are not available on the same LOR, but only nearby ones. This decoupling effect is similar to the ability of TOF discrimination to determine relative emission intensities along an LOR independently of attenuation.

The results in Fig 6 indicate that the algorithm is robust to a realistic amount of noise. Bias increases with added noise in the colder central region, but not significantly in the warmer peripheral regions.

Comparing the two source radii, we found very little difference in performance. With sTX there may be slightly better representation of the skull region at 150 mm (not shown) but it's a small effect. This is a fortunate result from an engineering perspective since it suggests there is considerable leeway on the placement of such sources in the gantry. The characteristics of an optimal sTX configuration are under investigation.

Based only on the relative attenuation of the emission and sTX 511 keV annihilation photons in the head, we estimate that such a source array might increase the absorbed gamma-ray dose to the patient's head by about 19% during the scan. If we further consider that the mean energy deposited by a positron emitted from one of the commonly used medical radioisotopes as it slows down in tissue is equal to or greater than 250 keV (the value for ^{18}F), then the relative increase in dose during the scan is likely $< 10\%$. However, since a brain scan typically lasts < 30 min, compared to the ^{18}F half-life of 110 min, the total increase in absorbed dose to the head in an ^{18}FDG clinical study would be $< 2\%$. The impact on whole-body effective dose would be much smaller, since the tissue weighting factor for the brain, as recommended by the ICRP [12] is only 0.01. Assuming the sTX sources are used only for a head scan and do not contribute significantly to the absorbed does in the rest of the body, the resulting increase in effective dose should be no more than $\approx 0.02\%$, which is negligible.

V. Conclusions

These simulations suggest that a simultaneous sparse transmission and emission measurement with joint reconstruction can give reasonably accurate compensation for attenuation in PET imaging of the head, and may thus be a viable alternative to CT-based attenuation correction for certain applications. Future work will examine the benefit of time-of-flight information for the measurement. Experimental verification is also in progress.

References

[1] M. Hofmann, B. Pichler, B. Schölkopf, and T. Beyer, "Towards quantitative PET/MRI: a review of MR-based attenuation correction techniques," *Eur J Nucl Med Mol Imaging*, vol. 36, pp. S93–S104, 2009.

[2] J. Nuyts, P. Dupont, S. Stroobants, R. Benninck, L. Mortelmans, and P. Suetens, "Simultaneous maximum a posteriori reconstruction of attenuation and activity distributions from emission sinograms," *IEEE Trans Med Imaging*, vol. 18, no. 5, pp. 393–403, May 1999.

[3] A. Martinez-Möller, M. Souvatzoglou, G. Delso, R. A. Bundschuh, C. Chefd'hotel, S. I. Ziegler, N. Navab, M. Schwaiger, and S. G. Nekolla, "Tissue classification as a potential approach for attenuation correction in whole-body PET/MRI: evaluation with PET/CT data," *J Nucl Med*, vol. 50, no. 4, pp. 520–526, Apr. 2009.

[4] V. Schulz, I. Torres-Espallardo, S. Renisch, Z. Hu, N. Ojha, P. Börnert, M. Perkuhn, T. Niendorf, W. M. Schäfer, H. Brockmann, T. Krohn, A. Buhl, R. W. Günther, F. M. Mottaghy, and G. A. Krombach, "Automatic, three-segment, MR-based attenuation correction for whole-body PET/MR data," *Eur J Nucl Med Mol Imaging*, vol. 38, no. 1, pp. 138–152, Jan. 2011.

[5] M. Hofmann, F. Steinke, V. Scheel, G. Charpiat, J. Farquhar, P. Aschoff, M. Brady, B. Schölkopf, and B. J. Pichler, "MRI-based attenuation correction for PET/MRI: A novel approach combining pattern recognition and atlas registration," *J Nucl Med*, vol. 49, no. 11, pp. 1875–1883, Nov. 2008.

[6] N. Burgos, M. J. Cardoso, K. Thielemans, M. Modat, S. Pedemonte, J. Dickson, A. Barnes, R. Ahmed, C. J. Mahoney, J. M. Schott, J. S. Duncan, D. Atkinson, S. R. Arridge, B. F. Hutton, and S. Ourselin, "Attenuation correction synthesis for hybrid PET-MR scanners: Application to brain studies," *IEEE Trans Med Imaging*, vol. 33, no. 12, pp. 2332–2341, Dec. 2014.

[7] C. C. Watson, "Supplemental transmission method for improved PET attenuation correction on an integrated MR/PET," *Nucl Instrum Methods Phys Res A*, vol. 734(B), pp. 191–195, Jan. 2014.

[8] H. Erdoğan and J. A. Fessler, "Joint estimation of attenuation and emission images from PET scans," *IEEE Nucl Sci Symp Conf Rec*, vol. 3, pp. 1672–1675, Oct. 1999.

[9] V. Y. Panin, M. Aykac, and M. E. Casey, "Simultaneous reconstruction of emission activity and attenuation coefficient distribution from TOF data, acquired with external transmission source," *Phys Med Biol*, vol. 58, no. 11, pp. 3649–3669, May 2013.

[10] S. Mustafovic and K. Thielemans, "Object dependency of resolution in reconstruction algorithms with interiteration filtering applied to PET data," *IEEE Trans Med Imaging*, vol. 23, no. 4, pp. 433–446, Apr. 2004.

[11] F. L. Andersen, C. N. Ladefoged, T. Beyer, S. H. Keller, A. E. Hansen, L. Højgaard, A. Kjær, I. Law, and S. Holm, "Combined PET/MR imaging in neurology: MR-based attenuation correction implies a strong spatial bias when ignoring bone," *NeuroImage*, vol. 84, pp. 206–216, 2014.

[12] A. D. Wrixon, "New ICRP recommendations," *J Radiol Prot*, vol. 28, pp. 161–168, 2008.